Highly Efficient Omnidirectional Integrated Multi-Band Wireless Energy Harvesters for Compact Sensor Nodes of Internet-of-Things

Highly Efficient Omnidirectional Integrated Multi-Band Wireless Energy Harvesters for Compact Sensor Nodes of Internet-of-Things

Chaoyun Song, *Member, IEEE,* Ping Lu, *Member, IEEE* and Shanpu Shen, *Member, IEEE*

***Abstract*— A novel highly-efficient radio-frequency (RF) energy harvester (rectenna) array with multi-frequency coverages (1.7–1.8 GHz and 2.1–2.7 GHz) as well as an omnidirectional 3D radiation pattern is presented. The harvester array is very compact and of low-profile, which strategically combines 12 single Vivaldi slot rectenna elements. More importantly, the proposed rectenna array is significantly simplified through a co-designed effective impedance tuning and array combination method to reduce the overall circuit complexity whilst maintaining high energy conversion efficiency (up to 67%) over the desired frequency band under different input powers (-25 to -5 dBm) and circuit loads (0.2 to 8 kΩ). Having utilized the proposed wireless energy harvester array, a complete system-level demonstration of ambient RF energy-powered, self-sustainable IoT sensor node is demonstrated for reliably operating in a typical indoor environment. Such a demonstration has never been reported before. In addition, the proposed rectenna array has novel features in terms of simplified Vivaldi rectenna matching, compact array combination and optimal beam shaping, which has proven to be an effective energy harvester in most domestic environments; therefore, having significant implications in powering small electronics for real-world Internal of Things (IoT) and Industrial Internal of Things (IIoT) applications.**

***Index Terms*— Energy harvesting, Internet of Things (IoT), radio-frequency, rectenna, wireless sensor nodes.**

Manuscript receive February 18, 2020, revised June 04, 2020, accepted July 02, 2020. This work was supported in part by the Heriot-Watt New Faculty Grant, in part by the National Natural Science Foundation of China (No. 51907130), in part by the Postdoctoral Science Foundation of China (No.20504153007), in part by the Sichuan Provincial Overseas Cooperation Grant (No. 2020YFH0091) and in part by the Fundamental Research Funds for the Central Universities (No.20504153015). (*Corresponding author: Ping Lu*).

C. Song is with the School of Engineering and Physical Sciences, Heriot-Watt University, Edinburgh EH14 4AS, Scotland, UK (e-mail: C.Song@hw.ac.uk).

P. Lu is with the School of Electronics and Information Engineering, Sichuan University, Chengdu 610064, China (email: pinglu90@scu.edu.cn).

S. Shen is with Department of Electronic and Computer Engineering, Institute for Advanced Study, Hong Kong University of Science and Technology, Hong Kong (e-mail: sshenaa@connect.ust.hk).

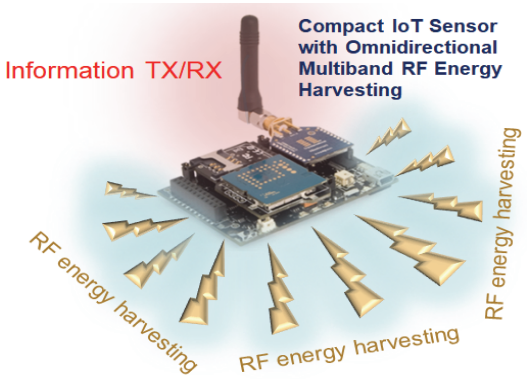

Fig. 1. Illustrative view of integrating multiband omnidirectional RF energy harvester array to a compact IoT sensor node. The RF energy harvester is produced on the outmost edges of the circuit board of the sensor system.

I. Introduction

EMERGING technologies such as the Internet-of-Things (IoT) highlight the significance of interconnecting vast numbers of smart objects (e.g., mobile devices and home appliances) equipped with wireless sensors to enable automation, real-time data monitoring and remote-control [1]-[3]. Powering millions of IoT sensors has been an open challenge since they typically need batteries that must be maintained, replaced and disposed (potential environmental pollutions). Therefore, self-powered, maintenance-free and low-cost devices are in high demand.

In recent years, a variety of energy sources such as solar, vibration, thermal and radio-frequency (RF) energies have been identified as potential solutions for powering these IoT sensors and devices [4]-[10]. Among all options, RF energy sources are becoming increasingly popular since they are ubiquitously available (e.g. from ambient Digital TV, mobile and WiFi signals) in most domestic environments regardless of the time, weather and environmental conditions [11]. A lot of industrial and academic research activities have been devoted to this field [12]–[17]. However, significant challenges have been found in the energy harvester (rectenna) designs. The main problem is that the existing technologies are not capable of harvesting sufficient energy over a wide ambient signal spectrum (e.g. from 0.8 to 5 GHz) and/or at the relatively low ambient power densities (i.e. $< 0.1\ \mu W/cm^2$) [18], [19].

Moreover, state-of-the-art broadband rectennas typically have a very complex structure and large size [20]. Thus, the energy capturing capability of current devices is relatively poor since it is costly and complicated to build effective rectenna arrays. Some efforts have been made to develop rectenna arrays. But most designs were reported for a single operating frequency band while the overall dimension of these arrays are large due to the essential spacing gap between the array elements. These examples include [21] and [22] for RF energy harvesting at the Wi-Fi band. More recently, some researchers have developed omnidirectional and multi-beam rectenna arrays in order to capture more energy from the randomly propagated wireless signals in multi-path ambient environments [23], [24]. However, these designs still have a limited frequency band coverage, and often of relatively high-profiles due to the spatial arrangements of the array. Only one broadband rectenna array using a single planar shape was reported in almost a decade ago [25]. But the overall energy conversion efficiency of this work was lower than 20%, which shows significant challenges in impedance matching for broadband rectennas. Moreover, some latest simplified broadband/multiband rectennas have demonstrated a high impedance conjugate matching system which may reduce the overall complexity and the total number of circuit components [26]-[28]. Unfortunately, they have only been investigated and demonstrated as a single rectenna.

In this paper, we present an omnidirectional multiband rectenna array design for ambient RF energy harvesting over frequency bands at 1.7–1.8 and 2.1 – 2.7 GHz. The rectenna array was strategically formed by using 12 Vivaldi slot rectennas for realizing a 3D omnidirectional radiation pattern with multiple beams and a reasonably high gain. The entire array is very compact and of low-profile, which outperforms the existing rectenna arrays using much complicated structures. In addition, the proposed rectenna array can be cooperatively integrated to any Printed Circuit Board (PCB)-based sensor devices within a single layer of circuit board (see Fig. 1). More importantly, the overall circuitry structure of the design is relatively simple where the antenna impedance is directly tuned to provide conjugate match with the rectifier input impedance over the frequency band of interest as well as under different input powers (-25 to -5 dBm) and load impedances (0.2 to 8 kΩ). The theoretical analysis and experiment validations of this novel impedance tuning method are presented. Finally, the harvested power from the rectenna array is utilized to power a commercial IoT sensor node in typical environments (signal power density between -40 and -60 dBm/cm^2). The complete energy harvester array has advantages in terms of simplicity, compactness, multi-beam, omnidirectional pattern and multi-band coverage compared with state-of-the-art designs.

The rest of this paper is organized as follows. The structure, performance, and design guidelines of the proposed broadband omnidirectional rectenna array is given in Section II. The experimental validations are presented in Section III. An example of integrating the proposed rectenna array to a commercial sensor node is discussed in Section IV. Finally, conclusions are drawn in Section V.

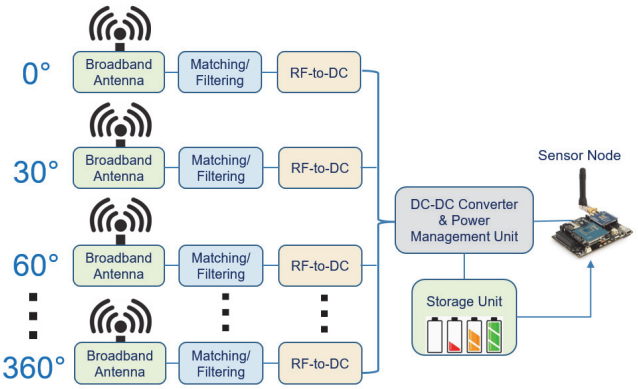

Fig. 2. Block diagram of the proposed omnidirectional broadband rectenna array and its application in charging a wireless IoT sensor node. There are 12 rectenna elements in total where each element has been configured to cover a 30° angular range over the entire horizontal plane from 0 to 360°.

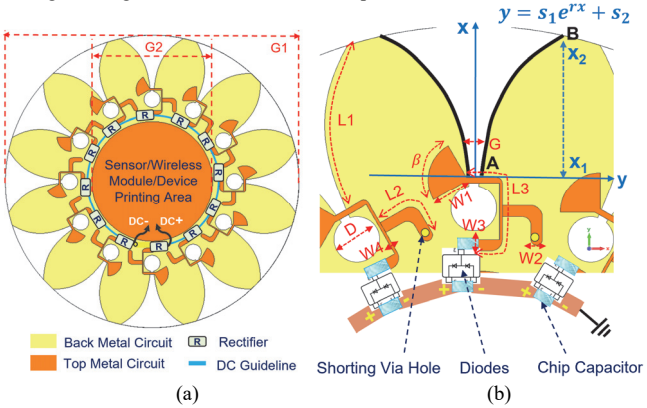

(a) (b)

Fig. 3. (a) Top view of the proposed omnidirectional rectenna array. (b) Enlarged view of a single Vivaldi slot rectenna element of the complete array. The details of the feeding strip (with marked notations) and the DC connection of the rectifier array are shown as well. The exponential taper profile of the Vivaldi slot is given.

TABLE I
GEOMETRIC PARAMETERS OF THE PROPOSED DESIGN

Parameter	G1	G2	G	L1	L2	L3
Value (unit: mm)	145	60	1.7	31.7	12.1	20.1
Parameter	W1	W2	W3	W4	D	β
Value (unit: mm)	6	2	2	0.5	4	65°

II. OMNIDIRECTIONAL INTEGRATED MULTIBAND RECTENNA ARRAY DESIGN

A. *Structure and Geometry*

The block diagram illustration of the proposed omnidirectional broadband rectenna array is given in Fig. 2. It consists of 12 wideband rectenna elements that are circularly connected as a loop. Each element is configured for an end-fire radiation with 30° beam coverage in the circular plane. The complete array could consequently realize an omnidirectional 3D radiation pattern that can efficiently harvest energy from any random incoming RF signals over a wide spectrum. In addition, the harvested energy is rectified by using RF-DC rectifiers and further regulated by using a DC-DC boost converter and power management unit (PMU) for charging a storage unit (e.g., super capacitor), or continuously powering the IoT sensors node.

This article has been accepted for publication in a future issue of this journal, but has not been fully edited. Content may change prior to final publication. Citation information: DOI 10.1109/TIE.2020.3009586, IEEE Transactions on Industrial Electronics

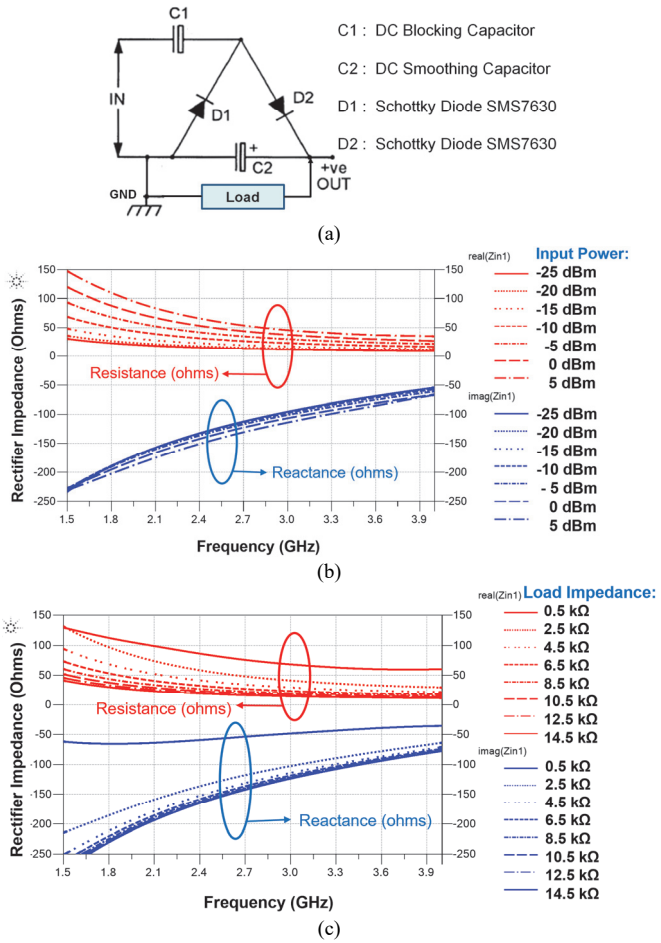

Fig. 4. (a) Schematic diagram of the rectifier used in this work. (b) Input impedance of the rectifier vs. frequency at different input power levels from -25 to 5 dBm. (c) Input impedance of the rectifier vs. frequency using different load resistances from 0.5 to 14.5 kΩ.

In order to develop a simplified energy harvester for PCB-based sensor devices, here we take the printing area for the senor devices and wireless modules into account (see Fig. 3 (a)). The complete rectenna array is produced on a single layer of PCB with a double-sided metallization. The substrate material is chosen as Rogers RT6002 with a relative dielectric constant of 2.94 and a thickness of 1.52 mm. The structural illustration of the detailed design is depicted Fig. 3 (a). The bottom layer acts as the circuit ground plane which is fully covered by metal. There are 12 Vivaldi-shaped slots cut on the outmost edge of the circular ground plane. On the top layer, the inner metal area has been configured for sensor and device printing. In addition, the Vivaldi slot is fed by using a U-shaped bent microstrip which is also printed on the top layer. In general, this design can be equivalently seen as a Vivaldi antenna array connected in a circular shape. Since it is known that Vivaldi antennas could exhibit broadband end-fire radiations [29], the proposed circularly connected Vivaldi slot antenna array will have an omnidirectional radiation pattern in the circular plane.

The enlarged view of the detailed feeding structure is shown in Fig. 3 (b). The U-shape bent microstrip is loaded with a radial stub on its open end. Meanwhile, a circular slot is also

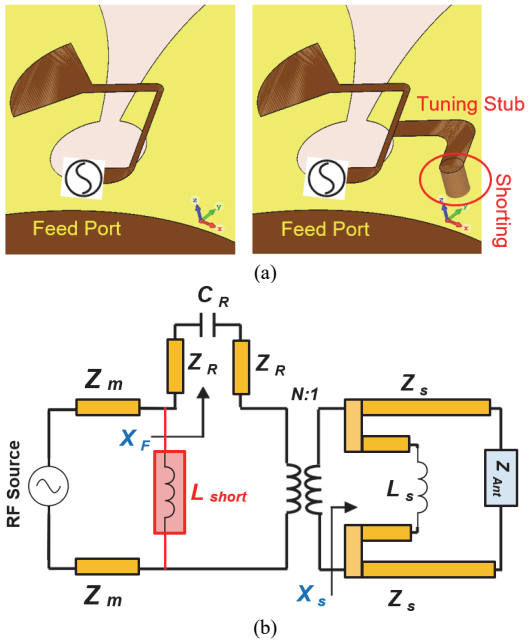

Fig. 5. (a) Illustration of the antenna feeding with and without using the impedance tuning stub (shorted by using via hole). (b) Equivalent circuit model of the proposed antenna with tuning stub.

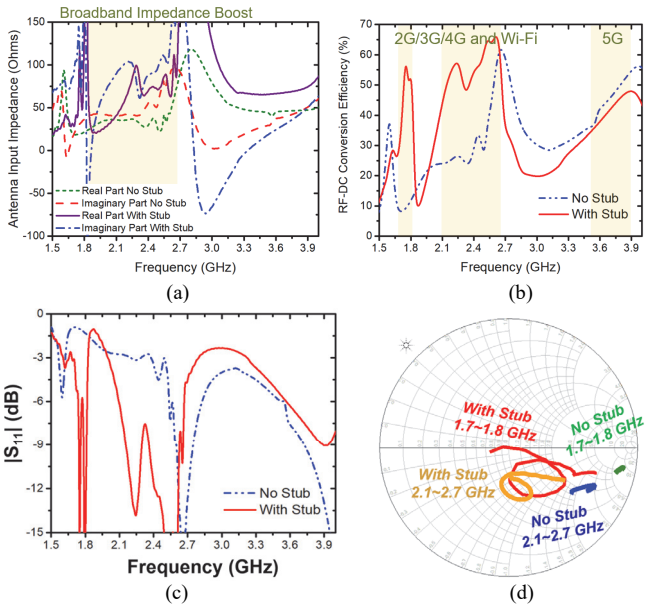

Fig. 6. (a) Simulated input impedance of a single Vivaldi slot antenna with and without using the impedance tuning stub. (b) Simulated RF-DC power conversion efficiency, (c) $|S_{11}|$ and (d) Smith chart of a single Vivaldi slot rectenna with and without using the impedance tuning stub. The circuit load is fixed at 2 kΩ and the input power is fixed at -3 dBm during the simulation.

loaded to the close end of the Vivaldi slot on the ground plane. Both loadings are aimed for getting the antenna impedance matched over a wide band. Importantly, an additional shorted stub is connected to the middle point of the U-shape feeding strip for broadband impedance tuning. The tuning mechanism of the proposed Vivaldi antenna will be introduced later. To design the shape of the slot, we use the exponential taper profile (see Fig. 3(b)) of the Vivaldi antenna, which is determined by the opening rate r and two points $A(x_1, y_1)$ and $B(x_2, y_2)$ [29], as given in (1).

This article has been accepted for publication in a future issue of this journal, but has not been fully edited. Content may change prior to final publication. Citation information: DOI 10.1109/TIE.2020.3009586, IEEE Transactions on Industrial Electronics

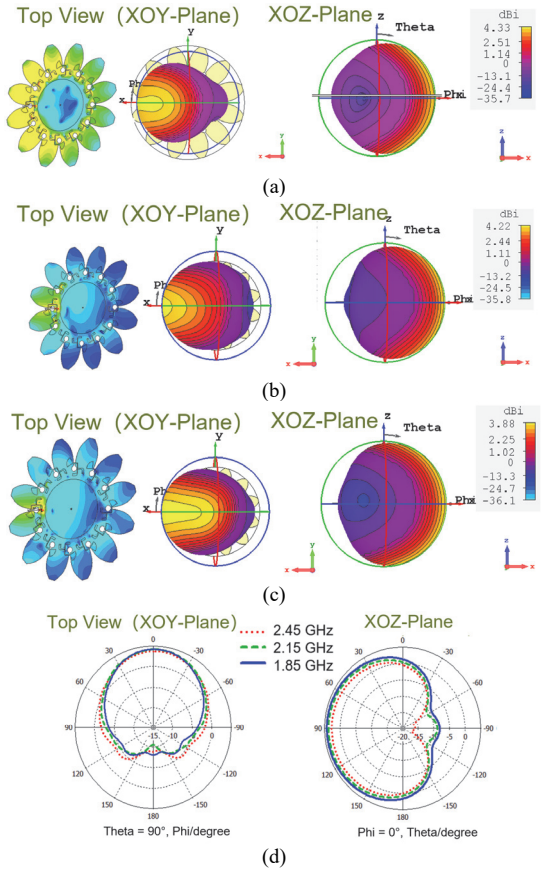

Fig. 7. 3D radiation patterns of a single Vivaldi slot antenna in top view and XOZ-plane view. (a) 1.8 GHz, (b) 2.15 GHz and (c) 2.45 GHz. The corresponding surface current distributions at these three frequencies are shown as well. (d) The normalized 2D patterns at three frequencies over XOY and XOZ plane.

$$y = s_1 e^{rx} + s_2 \tag{1}$$

where s_1 and s_2 can be written as:

$$s_1 = \frac{y_2 - y_1}{e^{rx_2} - e^{rx_2}} \tag{2}$$

$$s_2 = \frac{y_1 e^{rx_2} - y_2 e^{rx_1}}{e^{rx_2} - e^{rx_1}} \tag{3}$$

If the Vivaldi slot works at a low frequency mode, the end-fire radiation will have a very wide vertical beam-width which might be suitable for RF energy harvesting. Therefore, the size of the slot is designed to fulfil a quarter-wavelength (about 40 mm) radiator at 1.8 GHz. The opening rate r is set to 0.09 and the closing slot gap $G = 2\times S_2$ is set as 1.7 mm in this design. The optimized design parameters are given in Table I in which the overall dimension of the PCB is 145 × 145 × 1.53 mm^3 with a sensor printing area of 60 × 60 mm^2. It can be seen that the size of a single Vivaldi slot ($L1 + D$) is approximately 0.22 λ at 1.8 GHz. In the rectifier part, a voltage doubling rectifier [19], consisting of two chip capacitors and two SOT-23 packaged Schottky diodes SMS7630, is connected to the end of the feeding strip. The DC output of each rectifier is linked by using a metal strip where all DC storage capacitors are in a series connection.

B. Rectifier Analysis

Due to the nonlinearity of diode/transistor-based circuits, broadband impedance matching for rectifiers is typically very challenging to design. Therefore, it is important to get a clearer understanding on the rectifier impedance over a wide frequency band under different operating conditions in terms of input power and load impedance. The schematic of the proposed voltage doubling rectifier is shown in Fig. 4 (a). The rectifier was modelled and simulated using the ADS software. The Large Signal S-parameter (LSSP) simulator and Harmonic Balance (HB) simulator are employed to calculate the Z-matrix of the circuit. The simulated input impedance of the proposed rectifier versus a wide frequency band from 1.5 to 4 GHz is depicted in Fig. 4 (b) and (c) for different input power levels from -25 to 5 dBm and different load resistances from 0.5 to 14.5 kΩ, respectively. It can be seen that the real part of the impedance (resistance) varies between 150 and 10 Ω, while the imaginary part of the impedance (reactance) varies between -250 and -50 Ω under the aforementioned conditions. The rectifier exhibits significant capacitive impedance (reactance < 0 Ω) in a wide frequency band, which means that broadband inductive matching networks (or inductive antennas) are typically required to cancel the reactance of the rectifier. Therefore, the analysis in this section will be helpful to determine the optimal antenna impedance for broadband impedance matching during the antenna design.

C. Simplified Multiband Impedance Matching

Although Vivaldi slot rectennas have been previously reported [36], [37], their rectifier part still needs to use complex and multi-stage matching networks for realizing high RF-DC efficiency and enabling multiple frequency bands operation. Therefore, such conventional designs will not be suitable for expanding to rectenna arrays, especially for the tightly connected compact Vivaldi slot array as proposed here, in which the spaces for the rectifying circuit printing are very limited. In order to simplify the matching network and reduce the number of circuit components used in the design, here we will directly tune the antenna impedance for directly matching with the rectifier circuit over the frequency band of interest. Fig. 5 (a) shows the feeding structure of a conventional Vivaldi slot antenna as well as that of the proposed antenna by using an extra shorted impedance tuning stub. To understand the operation mechanism, we have built the equivalent circuit model of the proposed antenna by using that of an open-end shorted slot antenna [31] and Vivaldi antenna [32], as depicted in Fig. 5 (b). Herein, Z_m and Z_R represent the characteristic impedance of the microstrip feeding line and radial stub. Z_S and Z_{Ant} represent the characteristic impedance of the slot-line and Vivaldi antenna. The N: 1 transformer denotes the tapered structure and transition area of the Vivaldi slot. In addition, C_R is the equivalent capacitance of the radial stub over the ground plane while L_S represents the equivalent inductance of the close-end of the slot. In traditional Vivaldi antennas, C_R and L_S (radial stub and close-end of the slot) are specifically designed to cancel the reactance of the antenna for realizing a wideband impedance-matched travelling wave radiation. The reflection coefficient of the proposed Vivaldi antenna can be written as:

$$\Gamma_{Vivaldi} = \frac{R_T - Z_m - Z_R + j(X_F + X_T)}{R_T + Z_m + Z_R + j(X_F + X_T)} \tag{4}$$

This article has been accepted for publication in a future issue of this journal, but has not been fully edited. Content may change prior to final publication. Citation information: DOI 10.1109/TIE.2020.3009586, IEEE Transactions on Industrial Electronics

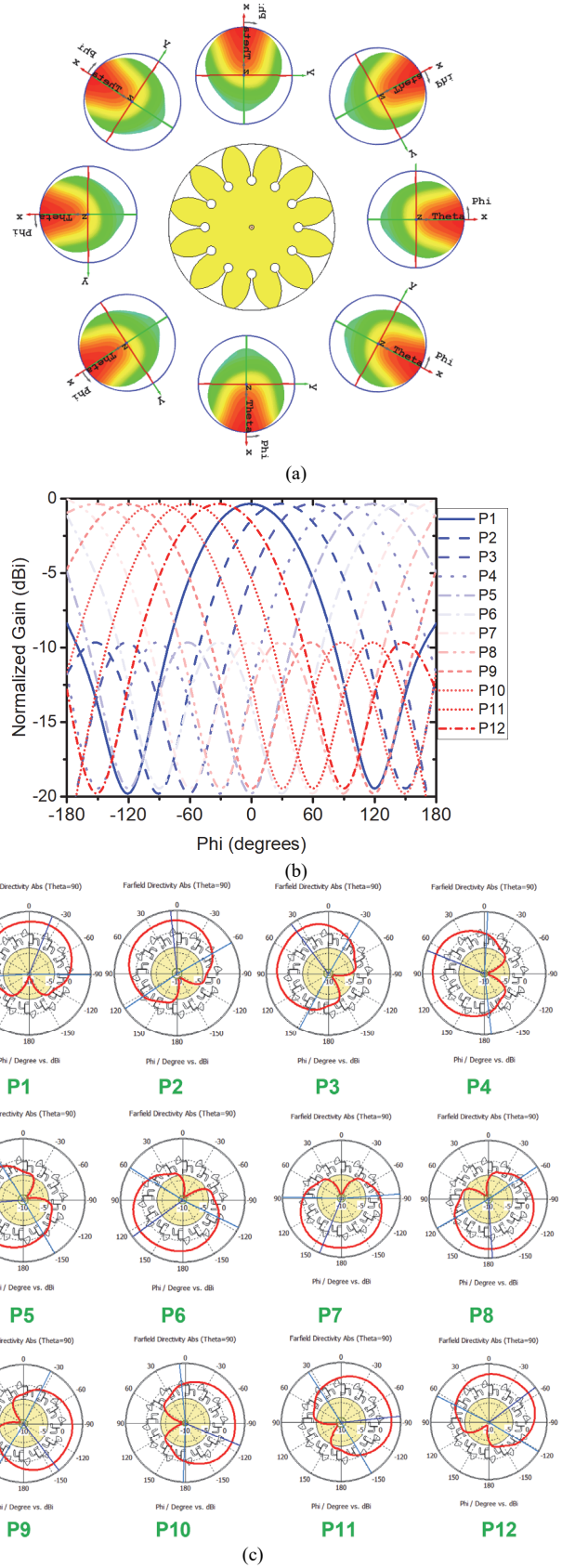

Fig. 8. (a) Illustration of the omnidirectional radiation pattern of the Vivaldi slot array over the horizontal plane (XOY-plane). (b) Cartesian plot and (c) Polar plot of Simulated 2D normalized gain pattern of the proposed 12 Vivaldi slot antennas over the XOY-plane (Theta = 90°, Phi = -180° to +180°).

where X_F represents the reactance of the feed line, whilst R_T and X_T (complex impedance of the Vivaldi slot antenna) can be further given by (assuming $Z_{Ant} = Z_S$)

$$R_T = N^2 \frac{Z_{Ant}X_S}{Z_{Ant}^2+X_S} \quad (5)$$

$$X_T = N \frac{Z_{Ant}X_S}{Z_{Ant}^2+X_S} \quad (6)$$

It can be seen that when X_F and X_T can be mutually cancelled, the antenna will have a matched impedance to a resistive port (e.g. 50 Ω) for wideband radiation. However, it is already shown from Section II-B that the proposed rectifier is of capacitive impedance. Therefore, a shorted tuning stub is added between the microstrip feed line and the radial stub. Such a stub can be modelled as a shunt inductor in the equivalent circuit (see highlighted L_{short} in Fig. 5 (b)), which could subsequently convert X_F to inductive reactance for cancelling the capacitive reactance of the proposed rectifier.

To validate the performance of this tuning stub, CST software was employed to model and optimize the antenna and tuning stub through a full-wave 3D electromagnetic (EM) simulation. The simulated input impedance of the single Vivaldi slot antenna element with/without using the tuning stub is shown in Fig. 6 (a). The conventional antenna has a flat impedance over 1.8 and 2.7 GHz, where the real part and imaginary part of the impedance are around 25 Ω and 30 Ω respectively (due to the reactance cancelation). Having added the tuning stub, the value of impedance is significantly increased over the frequency band of interest. The equivalent lumped-element circuit of the proposed tuning stub is a shunt inductor, hence it may enhance the value of the reactive part of the impedance via the means of inductive loading. As a result, the imaginary part of the impedance is increased to around 100 Ω over 2 to 2.4 GHz. Meanwhile, the real part of the impedance is also increased from 25 to 75 Ω in the desired frequency band after using the shorted stub. The antenna impedance is directly imported to the circuit model in the ADS by using the Data Access Component (DAC). In this scenario, the overall impedance matching performance of the complete rectenna can be obtained. By interconnecting the antenna and the simple rectifier as shown in Fig. 4 (a), the rectified DC voltage (V_{DC}) can be measured at the circuit load (R_L). Consequently, the RF-DC power conversion efficiency can be calculated using

$$\eta_{RF-DC} = \frac{V_{DC}^2}{R_L \times P_{RF}} \quad (7)$$

where P_{RF} is the received RF power by the antenna, or in other words, the input RF power to the rectifier. Since the source impedance of the circuit is set to the antenna impedance as depicted in Fig. 6 (a), the impedance mismatch of the complete system will be taken into consideration. An example of the simulated frequency dependence of the RF-DC power conversion efficiency of the proposed single Vivaldi rectenna element using the optimized tuning stub is given in Fig. 6 (b). The input power and load resistance are set to -3 dBm (0.5 mW) and 2 kΩ respectively. It can be seen that the proposed rectenna has achieved relatively high conversion efficiency (50 – 67%) over 1.7 – 1.8 and 2.1 – 2.7 GHz. Such a frequency coverage is desirable for RF energy harvesting as it covers the majority of

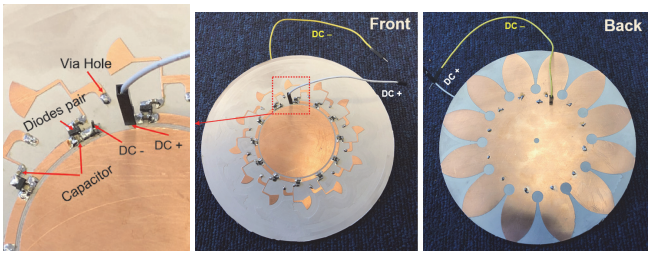

Fig. 9. Front and back view of the fabricated rectenna array prototype.

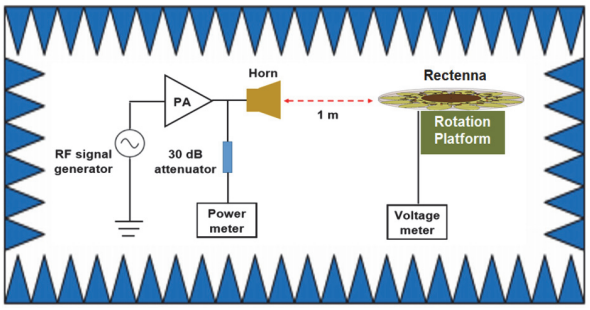

Fig. 10. Measurement setup and facilities of the proposed rectenna array.

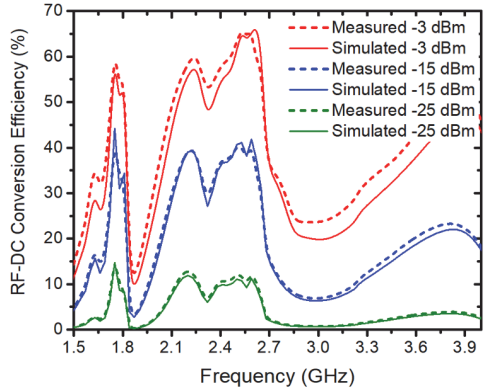

Fig. 11. Measured and simulated RF-DC conversion efficiency versus frequency at three different input power levels. The circuit load is fixed at 2 kΩ.

the 2G/3G/4G cellular bands as well as the WiFi/ISM 2.45 GHz bands. The reflection coefficient ($|S_{11}|$) and Smith Chart of the rectenna are given in Figs. 6 (c) and (d). It can be seen that the tuning stub has helped to cancel the capacitive reactance of the rectifier over 2.1 – 2.7 GHz and at around 1.8 GHz. As a comparison, the conventional design without using the tuning stub has obtained a poor matching performance ($|S_{11}|$ > -6 dB) and low RF-DC conversion efficiency over the frequency band of interest. It is demonstrated that the impedance of the Vivaldi slot antenna has been well-tuned to directly conjugate match with the rectifier impedance over a wide band.

It should be noted that the proposed tuning stub is different from the stubs used in conventional matching network design for antennas/rectifiers with 50 Ω port impedance. This stub has a major impact on the antenna impedance, i.e. converting the antenna reactance from non-inductive to inductive over a wide frequency band. Therefore, it is a novel impedance matching and antenna tuning method between two complex impedance ports with significant impedance validations versus frequency. This method could also be expanded for other non-50 Ω RF devices (e.g. RFID tags, antenna-on-chip) for simplified impedance matching.

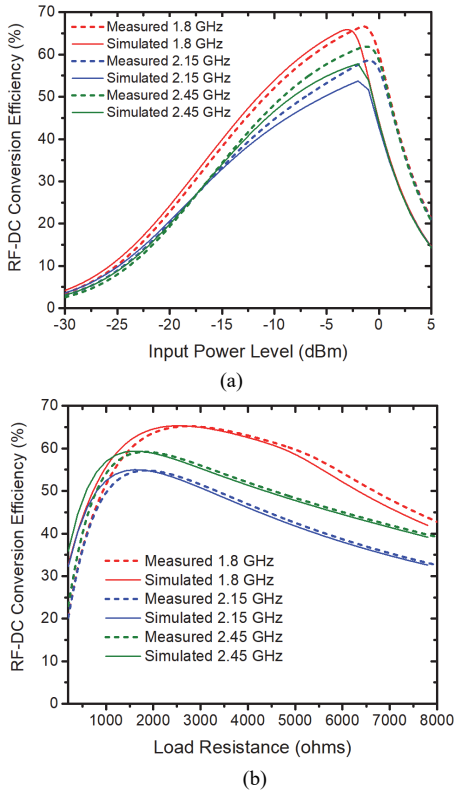

Fig. 12. Measured and simulated RF-DC conversion efficiency versus (a) input power level and (b) load resistance at three different frequencies. The circuit load for (a) is fixed at 2 kΩ and the input power for (b) is fixed at -3 dBm.

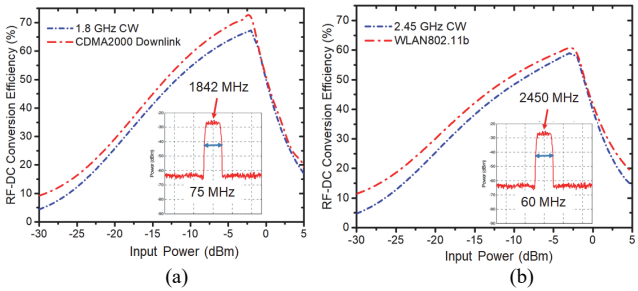

Fig. 13. Measured RF-DC conversion efficiency for (a) CW input signal at 1.85 GHz and CDMA downlink signals at 1.8 – 1.88 GHz. (b) CW input signal at 2.45 GHz and WLAN 802.11b signal at 2.42 – 2.48 GHz.

D. *Omnidirectional Array Performance*

To illustrate the omnidirectional array performance, we first study a single Vivaldi slot antenna where only one feeding port of the 12-slot array is excited. The simulated 3D radiation patterns at three different frequencies are depicted in Figs. 7 (a)-(c) along with the normalized 2D patterns in XOY-plane and XOZ-plane (see Fig. 7 (d)). It can be seen that the proposed antenna has achieved an end-fire radiation where the main antenna beam is targeted to the location of the excited Vivaldi slot. In addition, the antenna covers a wide beam-width over the XOZ plane at all three frequencies. The maximum gains and half-power beam-widths (XOZ-Plane) are about 4.33 dBi and 150° at 1.8 GHz, 4.22 dBi and 157° at 2.15 GHz, 3.88 dBi and 163° at 2.45 GHz, respectively. Moreover, the single Vivaldi antenna has realized a reasonable half-power beam width of around 60° in the XOY plane.

This article has been accepted for publication in a future issue of this journal, but has not been fully edited. Content may change prior to final publication. Citation information: DOI 10.1109/TIE.2020.3009586, IEEE Transactions on Industrial Electronics

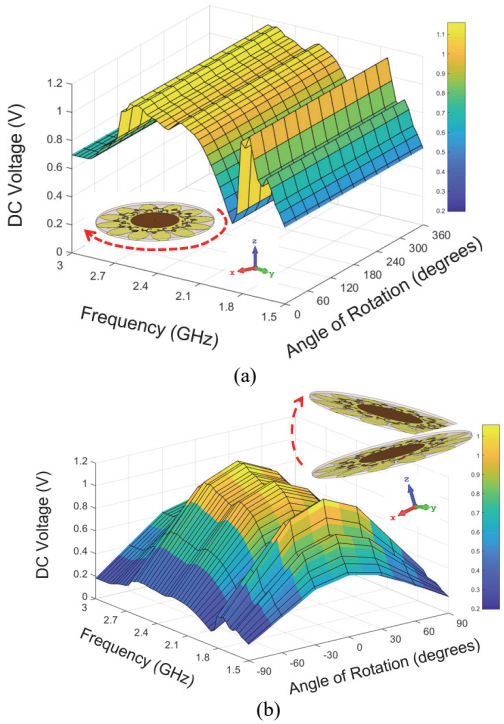

Fig. 14. Measured output DC voltage (a) versus frequency and 0 – 360° rotation angle in the XOY plane, (b) versus frequency and -90° to +90° rotation angle in the XOZ plane. The input power is fixed at -3 dBm.

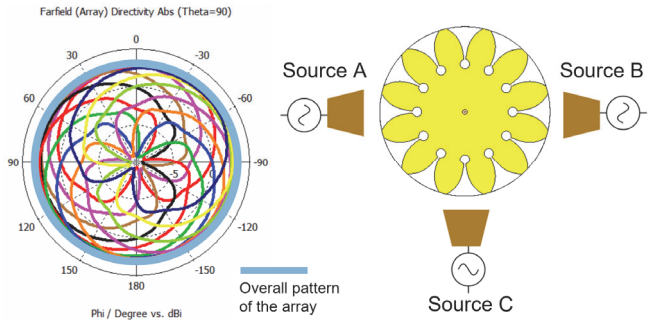

Fig. 15. (a) Measured overall received power pattern of the proposed rectenna in the XOY plane. (b) Measurement setup of harvesting energy from three RF sources at different locations. The frequency of RF source is fixed at 1.8 GHz.

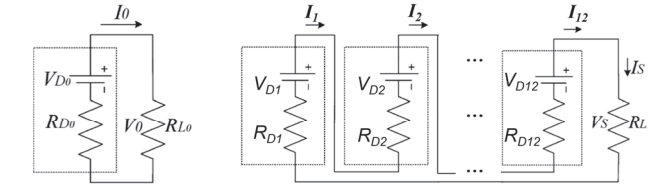

Fig. 16. Linear equivalent-circuit models of a single rectenna element and the complete rectenna array.

Next, all 12 feed ports of the proposed Vivaldi slot array are excited simultaneously. An illustration of the multi-beam scanning radiation pattern of the Vivaldi slot array over the horizontal plane (XOY-plane) is depicted in Fig. 8 (a). Furthermore, the simulated 2D normalized gain patterns of each individual port are given in Figs. 8 (b) - Cartesian plot and (c) - polar plot, respectively. It can be seen that the beam shape is almost maintained for different ports due to the high isolation between array elements for such tightly-connected Vivaldi slot array [29]. But the antenna beam direction is steered over the entire horizontal plane from -180° to +180°. Therefore, the proposed Vivaldi slot array could have a realized gain of > 3.5 dBi omnidirectionally in the horizontal plane and in a wide-angle range (150°) in the vertical plane, which makes it a multi-beam, quasi-3D omnidirectional RF energy harvester.

III. PROTOTYPE FABRICATION AND EXPERIMENTAL VALIDATIONS

The proposed Vivaldi rectenna array has been fabricated and measured. A picture of the fabricated prototype is given in Fig. 9. The chip capacitors were 100 nF SMD capacitors from Murata. The rectifying diodes was SMS7630 Schottky diodes in a SOT-23 package provided by Skyworks Inc. It has been previously shown that SMS7630 has a very low forward bias voltage of 0.15 ~ 0.25 V and meanwhile has a relatively high saturation current of 5 μA. In addition, the junction capacitance and series resistance of the product is 0.14 pF and 20 Ω [19]. Overall, it exhibits the smallest power consumption and lowest start-up voltage among existing commercial products, which is very suitable for low power-density RF energy harvesting applications. The measurement setup is depicted in Fig. 10 where the signals generated by an RF signal generator were amplified by a 30-dB gain power amplifier (PA) and transmitted by a calibrated horn antenna R&SHF906. The proposed rectenna was used to receive the signal at a distance of 1 m from the transmitting horn antenna. The transmitting power was measured by a power meter, while the received power by the rectenna was calculated by using the Friis equation

$$P_r = P_t + G_t + G_r + 20\log_{10}\frac{\lambda}{4\pi D} \quad (8)$$

where P_r is the input RF power to the rectifier in dBm, P_t is the transmitting power of the horn in dBm, G_t is the realized gain of the horn in dBi, Gr is the realized gain of the proposed rectenna in dBi, λ is the wavelength of interest, and D is the distance (D = 1 m).

A. Energy Conversion Efficiency at Fixed Incident Angles

First of all, the rectenna array was tested at a fixed incident angle. In this scenario, only one Vivaldi slot rectenna was connected to the DC output and measured. It is worth noting that the antenna orientation over the frequency band of 1.5 – 4 GHz was tuned to match with its maximum beam direction during the measurement (in order to avoid additional power loss). By using (5), the required transmitting RF power can be calculated for realizing a stable received power level over a wide frequency band. The proposed rectenna array was tested at three different received power levels which are -25 dBm, -15 dBm and -3 dBm respectively. Such an input power range could represent the typical ambient RF signals that normally have a low power density (-40 to -60 dBm/cm^2). Also, most Schottky diode-based rectifier cannot work well for < -30 dBm input power [19]. From Fig. 11, it can be seen that the measured and simulated RF-DC conversion efficiency agreed reasonably well, where the average efficiency over the desired wide band of 1.7 – 1.8 and 2.1 – 2.7 GHz is above 50% (up to 66%) at -3

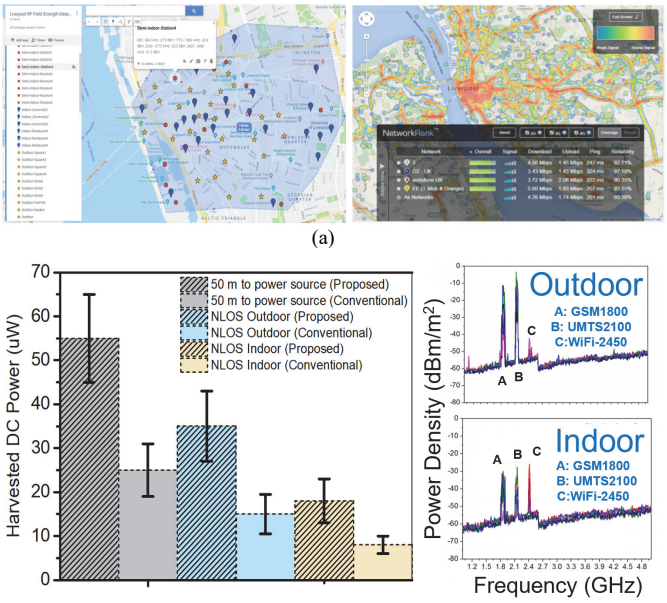

Fig. 17. (a) Test locations in real-world ambient urban environments. The locations are selected using (https://www.opensignal.com/networks). (b) Measured average harvested DC power from three different types of locations. The comparison between the proposed omnidirectional multiband rectenna array and a single broadband rectenna is shown. (c) Examples of measured typical outdoor and indoor ambient signal strength from 1.2 to 4.8 GHz (please note the unit of power density in this figure is dBm/m^2).

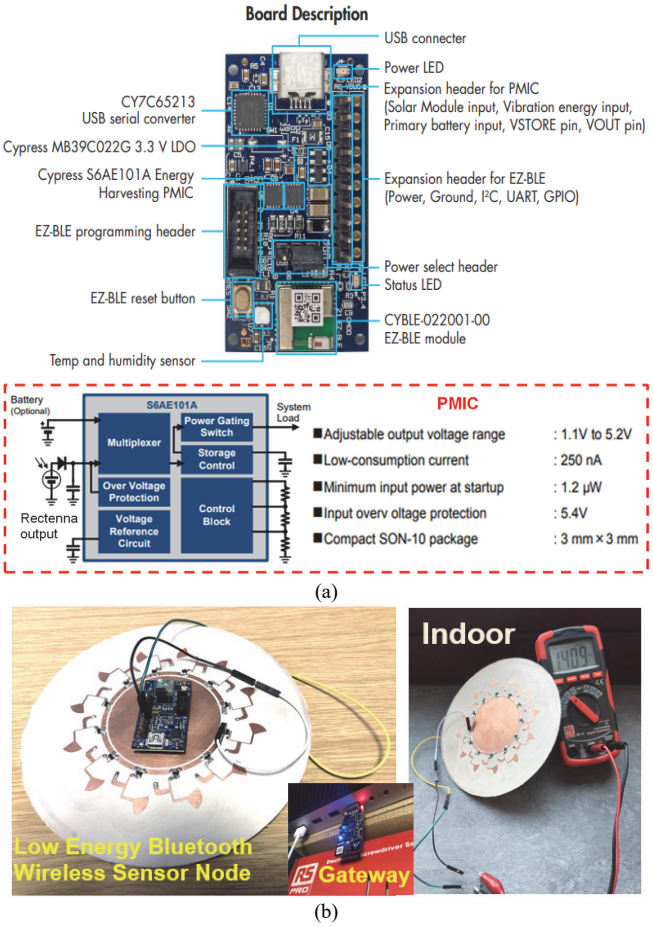

Fig. 18. (a) Top view and board description of Cypress IoT sensor node. The details of the PMIC are provided by [30]. (b) Example of powering the wireless sensor node by using the proposed RF energy harvester. The data was received by using an USB gateway.

dBm, 30% (up to 40%) at -15 dBm, and 5% (up to 13%) at -25 dBm respectively. In addition, if the input power is varied between -30 dBm and 5 dBm, the conversion efficiency at three major resonant frequencies is depicted in Fig. 12 (a). It can be seen that the overall efficiency of this design is comparable with that of other wideband low-power rectennas. The peak efficiency (68% at 1.8 GHz) is achieved at around -3 dBm input power. Lastly, it can be seen from Fig. 12 (b) that the proposed rectenna has a relatively stable efficiency over a wide circuit load range from 200 to 8000 Ω. This shows that the proposed rectenna could be integrated with different load devices.

The rectenna was also tested for receiving modulated waves to match the realistic signal conditions in the ambient environment. The Keithley2920 RF signal generator was used to transmit CDMA downlink (spectrum: 1.8 – 1.88 GHz) and WLAN802.11b (spectrum: 2.42 – 2.48 GHz) signals using the setup in Fig. 10. The results of conversion efficiency vs. input power of these modulated waves are given in Fig. 13 and compared with that of the continuous wave (CW) at 1.8 and 2.45 GHz. It can be seen that the rectenna has a higher efficiency for the modulated input signals, which is due to an enhanced power integration over the modulated signal spectrum [33]. Therefore, the proposed rectenna may have an improved efficiency in realistic energy harvesting environment with various modulated signals.

B. Omnidirectional Energy Harvesting Performance

Secondly, a 3D rotation platform is introduced for the measurement system (as shown in Fig. 10). During the measurement, all DC output capacitors of the Vivaldi rectenna array were connected serially. The proposed rectenna array was firstly rotated horizontally from 0° to 360° (over XOY plane as shown in Fig. 14 (a)). The rectified DC voltage was recorded in the frequency band of 1.5 to 4 GHz (0.1 GHz step width) for a constant -3 dBm received RF power. It can be seen that the measured DC voltage is relatively stable across the desired band of 1.7 – 1.8 GHz and 2.1 – 2.7 GHz. More importantly, the voltage is almost constant with no ripples during the physical rotation over the horizontal plane (see Fig. 14(a)). In addition, if the rectenna array was rotated over the vertical plane (XOZ plane in Fig. 14(b)), the output voltage is maintained stably for a wide angle range from -60° to 60°. At the peak voltage output (1.1 V), the corresponding overall energy conversion efficiency is about 65% (3500 Ω load). The overall normalized received power pattern of the complete array is given in Fig. 15 (a) along with the patterns of 12 single rectenna elements in the XOY plane. It can be seen that the overall pattern of the array is almost a perfect circle. This has confirmed that the proposed rectenna array can efficiently harvest wideband RF signals in an omnidirectional 3D angle range.

C. DC Combination of the Rectenna Array

The output DC power of the proposed rectenna array is serially combined (voltage combination), as shown in Fig. 3 (layout) and Fig. 9 (prototype). Therefore, it is worth to

This article has been accepted for publication in a future issue of this journal, but has not been fully edited. Content may change prior to final publication. Citation information: DOI 10.1109/TIE.2020.3009586, IEEE Transactions on Industrial Electronics

investigate the effect of the DC combination network and multiple dynamic DC output powers from different rectenna elements. Although the rectenna is a nonlinear device, for simplicity and easy analysis, we have built the linear equivalent circuit models of a single rectenna and the proposed rectenna array, as depicted in Fig. 16, where $R_{D0\text{-}D12}$ represents the rectenna element impedance while R_{L0} and R_L are the load resistance of single element and the complete array respectively. According to [35], the output power can be written as

$$\text{Single element: } P_0 = \frac{V_{D0}^2 R_{Lo}}{(R_{D0}+R_{Lo})^2} \quad (9)$$

$$\text{Rectenna array: } P_s = \frac{(\sum_{n=1}^{12} V_{Dn})^2 R_L}{(\sum_{n=1}^{12} R_{Dn}+R_L)^2} \quad (10)$$

If we assume all rectenna elements are identical, for the maximum power output condition, the load impedance of the array should be $R_L = n \times R_{L0}$, where R_{L0} is the load impedance of a single element and *n* is the number of elements [35]. Due to the limited number of RF sources and TX antennas in our lab, here we show an example of using the proposed rectenna array to harvest incoming signals from three RF power sources (1.8 GHz) at different incident angles (see Fig. 15(b)). The measurement procedure is given as below:

1) We disconnected the array by removing unused diodes and tested the DC power separately at the outputs of three single rectenna elements with three RF input signals from different directions (A, B and C). The load impedance of each element was 2000 Ω. The received RF power of each element was configured at 100 μW (-10 dBm) by using (8).
2) The three rectenna elements were serially connected and tested with simultaneous RF inputs from sources A, B and C. Based on the analysis in (9)-(10), the total load resistance used for the array was tripled in this case (6000 Ω).
3) Repeat steps (1) and (2) by using dynamic input RF power, the received power from sources A, B, and C was configured at 32 μW (-15 dBm), 100 μW (-10 dBm) and 320 μW (-5 dBm) respectively.

The measured output DC power from single rectenna elements and the rectenna array is given in Table II (texts in red color represent the results for dynamic output DC powers from the rectenna elements). The DC power combining efficiency is calculated using the total output DC power divided by the sum of the DC powers from three single elements. It can be seen that the DC power combining efficiency for three identical input powers at -10 dBm of each is about 94% (6% loss). While the efficiency is reduced to 86% [235 μW/(208+52+13.2) μW] when the received RF power from the RF sources is dynamically changed from -15 to -5 dBm. This is due to the nonlinear effect of the rectenna elements in which the RF-DC conversion efficiency and impedance matching efficiency typically vary as a function of load impedance and input power levels. To further improve the DC combining efficiency, multiple input and multiple output (MIMO) DC-DC switching converters can be used to replace the conventional resistors and match all the rectifiers to their optimal load [18], [19].

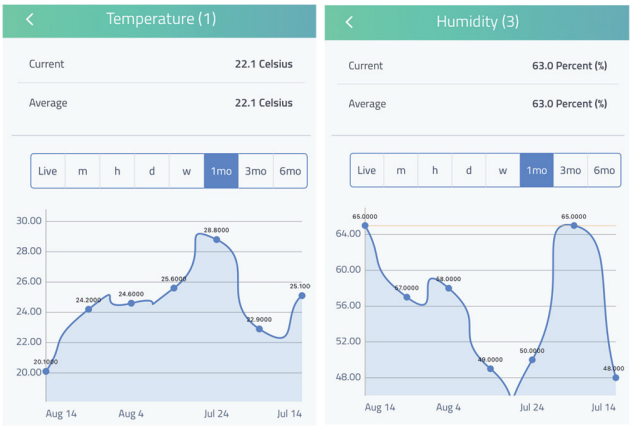

Fig. 19. Continuous monitoring of ambient temperature and humidity by using the proposed energy-harvesting wireless sensor node. The real-time data is visualized using Cayenne mobile app.

TABLE II
MEASURED DC POWER COMBINATION PERFORMANCE

	Input RF power	Output DC power	RF-DC efficiency	DC Combining efficiency*
Single element for source A	100 μW 32 μW	54 μW 13.2 μW	54% 41.5%	100% 100%
Single element for source B	100 μW 100 μW	52 μW 52 μW	52% 52%	100% 100%
Single element for source C	100 μW 320 μW	53.7 μW 208 μW	53.7% 65%	100% 100%
Three elements array for source A+B+C	**300 μW** **452 μW**	**150 μW** **235 μW**	**50%** **52%**	**94%** **86%**

D. *Test in Real Ambient Environments*

We have also conducted some measurements in real ambient environments. Fig. 17 (a) illustrates the 30 measurement locations in the city area of Liverpool in the United Kingdom. There are three different categories including: 1) 50 meter line-of-sight (LOS) to the mobile base-stations (power sources); 2) non line-of-sight (NLOS) to power sources in typical outdoor urban environments and 3) NLOS to power sources in typical office environments. Please note the locations are selected in accordance with the latest UK mobile coverage heat map (https://www.opensignal.com/networks) to ensure good RF signal strengths and avoid dead spots. These three aforementioned cases may represent the high, medium and low power density cases for ambient RF signals in most urban and domestic areas. By recording the output voltage from the rectenna array, the harvested DC power can be obtained. The average harvested power of the three cases is given in Fig. 17 (b) with error bars. As a comparison, the harvested power from the proposed omnidirectional multiband Vivaldi rectenna array as well as that from the conventional single broadband Vivaldi rectenna element (by disconnecting other array elements) is depicted in the figure. It can be seen that the proposed array can harvest around 55 μW (which is 30 μW higher than the power from a single element) when the location is about 50 m to mobile base stations. Secondly, if the test location is changed to typical outdoor urban environments (NLOS to power sources), the ambient power density could be

TABLE III
COMPARISON OF THE PROPOSED RECTENNA ARRAY AND RELATED DESIGNS

Ref. (year)	Impedance bandwidth (GHz)	FBW*	Number of array elements	Overall complexity	Overall dimension of the complete rectenna array	Maximum conversion efficiency	Input power level /load resistance range of interest	Measured harvested DC power vs. typical ambient power densit
[20] (2019)	0.93 – 0.95, 1.8 – 1.86	3.2%, 3.3%	16	Complex	240 mm × 240 mm × 22 mm	58% at -5 dBm	-30 to 0 dBm /14 and 28 kΩ	22 uW @ -13 dBm/cm^2 (outdoor)
[21] (2012)	2.38 – 2.5	4.9%	9	Complex	90 mm × 90 mm × 9.4 mm	67% at -5 dBm	-30 to 0 dBm /10 kΩ	5 uW @ -40 dBm/cm^2 (indoor)
[24] (2019)	2.4 – 2.43	1.2%	16	Complex	260 mm × 260 mm × 290 mm	45% at -5 dBm	-30 to 0 dBm /5.1 kΩ	4 uW @ -40 dBm/cm^2 (indoor)
[34] (2019)	1.84, 2.14, 2.45	3%	16	Complex	200 mm × 200 mm × 101.4 mm	60% at -5 dBm	-30 to -5 dBm /5 kΩ	63 uW @ -13 dBm/cm^2 (outdoor)
This work (2019)	**1.7 – 1.8, 2.1 – 2.7**	**5.8%, 25%**	**12**	**Simplest**	**145 mm × 145 mm × 1.53 mm**	**67% at -3 dBm**	**-30 to 0 dBm /from 1 to 6 kΩ**	**65 uW @ -13 dBm/cm^2 (outdoor) 20 uW @ -40 dBm/cm^2 (outdoor)**

*FBW: Factional Bandwidth

smaller which results a reduced harvested DC power of 35 µW for the array (17 µW for a single element). Lastly, the power density of ambient RF signals could be even lower in indoor environments due to a strong multi-path fading effect. Consequently, the harvested power by the array is reduced to 20 µW, but as a comparison, a single wideband rectenna element can only obtain less than 10 µW power in this scenario. An example of the measured typical indoor and outdoor ambient signal spectrum and strength are depicted in Fig. 17 (c). The spectrum power density levels are about -5 to -10 dBm/m^2 (-45 to -50 dBm/cm^2) and -25 to -30 dBm/m^2 (-65 to -70 dBm/cm^2) in outdoor and indoor environments, respectively. The total harvested RF power by the proposed rectenna array can be written as

$$P_{RF-Total} = \sum_{n=1}^{12} \int_{\theta}^{\theta'} \int_{f}^{f'} P_n \, d\theta df \quad (11)$$

$$P_n = \frac{\lambda^2 G}{4\pi} \times S \quad (12)$$

where P_n is the power received by a single antenna element (the *n-th* element), λ is the wavelength, G is the realized gain and S is the power density. In addition, the integral functions over $\theta - \theta'$ and $f - f'$ represent the power integration over the frequency bands and incident angles. Therefore, the proposed rectenna can harvest integrated/combined wideband RF power omnidirectionally. Thanks to the wide-area coverage and multi-path propagation of RF signals in urban environments, the proposed omnidirectional array could capture more power than other conventional unidirectional rectenna arrays and/or single rectenna element.

IV. INTEGRATION ON COMPACT IOT SENSOR NODES

In this section, a design example will be given to demonstrate the feasibility of integrating the proposed rectenna array to commercial IoT sensor nodes. Ideally, the circuit schematics for the sensors and wireless modules can be directly produced on the inner device printing area of the proposed rectenna array. In this case, the functions of the IoT sensor node and RF energy harvesting can be cooperatively integrated. More importantly, the complete product can be printed on a single layer of PCB which might be advantageous for industrial volume productions. For simplicity, here we select an off-the-shelf wireless IoT sensor node which is developed by Cypress [30]. The top view of the circuit and the board description of the proposed sensor node is given in Fig. 18 (a). It is worth noting that this sensor node product has been already installed with a built-in energy harvesting power management integrated circuit (PMIC). This PMIC has a minimum startup power of only 1.2 µW and a very low consumption current of 250 nA during the operation. On the other hand, it can boost a low input voltage from 0.1 V to an adjustable output voltage level between 1.1 and 5.2 V. The efficiency of the DC-DC boost converter of the PMIC starts from 30% (at 0.1 V input voltage) to the saturated level of 90% (for 2 V input voltage and above). Therefore, such PMICs are particularly suitable for low power energy harvesting applications. The details of the PMIC including the block diagram of functional parts and the recommended input parameters are given in Fig. 18 (a) as well. In addition, the selected IoT sensor node has been installed with on-board temperature and humidity sensors. The radio module of the product is a long-distance Bluetooth Low-Energy (BLE) wireless module (CYBLE-022001-00: EZ-BLE™ Creator Module). Overall, the power consumption of this sensor node is about 5 µW for standalone operation and 0.4 mW during radio transmissions. The data can be received by using an USB gateway with a sensitivity down to -110 dBm. Generally, the recommended wireless communication distance should be within 30 meters for this application. Fig. 18 (b) shows that the proposed IoT sensor node has been integrated to the proposed omnidirectional multiband RF energy harvester. In a typical indoor environment (with lower power densities), the output voltage from the rectenna array is normally around 0.1 – 0.2 V while the harvested power is between 15 and 25 µW, which is sufficient for the standalone operation of sensors. The DC-DC boost efficiency was about 30% (at 0.13 V input) for the indoor

wireless energy harvesting while the efficiency will go up to 80% for outdoor cases where the input voltage from the harvester was about 0.9 V. The overall energy demand of the proposed BLE sensors was estimated as 233.4 μJ, therefore the minimal capacity of the storage unit (super capacitor) was calculated as 67.8 μF to support the reliable operation of the BLE sensor system whilst maintaining reasonable charging time. According to the recommended operating condition of the PMIC used in this work, the on-board storage capacitor was chosen to be 100 μF. However, for applications with a larger energy consumption, the capacitor size will need to be increased substantially to meet the operation requirement. In this work, we have programmed the sensor device to set a data transmission interval of 30 minutes. Meanwhile, the sensor node will work in a deep-sleep mode with very low power consumptions during the non-transmission period. The harvested energy will be stored in an internal storage unit which is also managed by the PMIC. Most of the saved energy will be consumed for sending the data in every 30 minutes.

We have embedded the received data to an online Cloud platform named Cayenne, which also supports mobile App data visualizations. Fig. 19 depicts an example of continuous monitoring of the room temperature and humidity over a calendar month from July 14th to August 14th, 2019. The sensor node works alone during daytime and night time without the need for external batteries. The harvested RF energy is sufficient to support such low-power IoT applications, which could be further exploited for smart home monitoring and control etc. Please note that the presented design using BLE technology is just an example to show the feasibility of the proposed RF energy harvester in such IoT applications. Other long-range and low power sensor nodes using alternative communication technologies such as LoRaWAN and NB-IoT could also be considered and employed for developing similar energy-harvesting IoT products.

The performance comparison between the proposed rectenna array and other related rectenna arrays and multiport designs is depicted in Table III. It can be seen that our work covers the widest frequency bandwidth among the existing work. In addition, the overall energy conversion efficiency at low power levels from -30 to 0 dBm is comparable with the state-of-the-art results. More importantly, the proposed design has achieved a very simple structure (no complex matching networks and antenna structures) and very low profile (single PCB layer and compact array combination), compared with state-of-the-art multiband and multidirectional energy harvester arrays [34]. In addition, we have compared the output DC power from the proposed wireless energy harvester with the published work at the similar ambient power densities. To make a fair comparison, we chose -13 dBm/cm^2 and -40 dBm/cm^2 as the threshold for representing the typical outdoor and indoor RF power densities. From Table III, it can be seen that the proposed rectenna array has realized almost the highest output power using a smaller overall antenna size and circuitry dimension. Evidently, we have produced a much-simplified energy harvester design which is suitable for powering real-world small electronic devices and for volume production of real-world IoT sensor nodes with an embedded RF energy harvesting system at a low cost.

V. Conclusion

An omnidirectional multiband RF energy harvester array has been presented both theoretically and experimentally, which realized relatively high energy conversion efficiency (up to 67%) over the frequency bands of 1.7 – 1.8 GHz and 2.1 – 2.7 GHz, as well as a very compact size (tightly connected Vivaldi array) and low profile (1.53 mm thickness). The overall design has been simplified through a novel impedance tuning and rectenna array co-design technique. In addition, the proposed rectenna has an omnidirectional pattern with multi-beam and average gain > 3.5 dBi. It can capture significantly enhanced power from the ambient RF signals compared with the state-of-the-art ambient wireless energy harvesters; therefore, has proven to be an effective energy harvester in most domestic environments. As a potential real-world product demonstration, we have also presented a compact low-power IoT sensor example using the proposed highly-integrated RF energy harvester array, which showed standalone, long-term and self-powered operation in 24 hours without the need of battery replacements over calendar months. The proposed multiband, multibeam scanning, and omnidirectional energy harvester has outstanding performance in term of simplicity and compactness; therefore, it can be effectively applied to various IoT and IIoT applications.

References

[1] A. Zanella, N. Bui, A. Castellani, L. Vangelista and M. Zorzi, "Internet of Things for Smart Cities," *IEEE Internet of Things Journal*, vol. 1, no. 1, pp. 22-32, Feb. 2014.

[2] L. D. Xu, W. He and S. Li, "Internet of Things in Industries: A Survey," *IEEE Transactions on Industrial Informatics*, vol. 10, no. 4, pp. 2233-2243, Nov. 2014.

[3] M. Chiang and T. Zhang, "Fog and IoT: An Overview of Research Opportunities," *IEEE Internet of Things Journal*, vol. 3, no. 6, pp. 854-864, Dec. 2016.

[4] Y. K. Tan and S. K. Panda, "Energy Harvesting From Hybrid Indoor Ambient Light and Thermal Energy Sources for Enhanced Performance of Wireless Sensor Nodes," *IEEE Trans. Ind. Electron.*, vol. 58, no. 9, pp. 4424-4435, Sept. 2011.

[5] J. J. Estrada Lopez, A. Abuellil, A. Costilla Reyes, M. Abouzied, S. Yoon and E. Sanchez-Sinencio, "A Fully Integrated Maximum Power Tracking Combiner for Energy Harvesting IoT Applications," *IEEE Trans. Ind. Electron.*. In press, 2019.

[6] T. Hosseinimehr and A. Tabesh, "Magnetic Field Energy Harvesting from AC Lines for Powering Wireless Sensor Nodes in Smart Grids," *IEEE Trans. Ind. Electron.*, vol. 63, no. 8, pp. 4947-4954, Aug. 2016.

[7] Z. J. Chew and M. Zhu, "Adaptive Self-configurable Rectifier for Extended Operating Range of Piezoelectric Energy Harvesting," *IEEE Trans. Ind. Electron.*. in press, 2019

[8] M. R. Elhebeary, M. A. A. Ibrahim, M. M. Aboudina and A. N. Mohieldin, "Dual-Source Self-Start High-Efficiency Microscale Smart Energy Harvesting System for IoT," *IEEE Trans. Ind. Electron.*, vol. 65, no. 1, pp. 342-351, Jan. 2018.

[9] L. Guo, X. Gu, P. Chu, S. Hemour and K. Wu, "Collaboratively Harvesting Ambient Radiofrequency and Thermal Energy," *IEEE Trans. Ind. Electron.*.in press, 2019.

[10] V. Duong, N. X. Hieu, H. Lee and J. Lee, "A Battery-Assisted Passive EPC Gen-2 RFID Sensor Tag IC With Efficient Battery Power Management and RF Energy Harvesting," *IEEE Trans. Ind. Electron.*, vol. 63, no. 11, pp. 7112-7123, Nov. 2016.

[11] S. Kim et al., "Ambient RF energy-harvesting technologies for selfsustainable standalone wireless sensor platforms," *Proc. IEEE*, vol. 102, no. 11, pp. 1649–1666, Nov. 2014.

[12] K. Niotaki, A. Collado, A. Georgiadis, S. Kim, and M. M. Tentzeris, "Solar/electromagnetic energy harvesting and wireless power transmission," *Proc. IEEE*, vol. 102, no. 11, pp. 1712–1722, Nov. 2014.

[13] V. Palazzi et al., "A novel ultra-lightweight multiband rectenna on paper for RF energy harvesting in the next generation LTE bands," *IEEE Trans. Microw. Theory Tech*., vol. 66, no. 1, pp. 366–379, Jan. 2017.

[14] C. Song et al., "A novel six-band dual CP rectenna using improved impedance matching technique for ambient RF energy harvesting," *IEEE Trans. Antennas Propag*., vol. 64, no. 7, pp. 3160–3171, Jul. 2016.

[15] C. Song, Y. Huang, J. Zhou, J. Zhang, S. Yuan, and P. Carter, "A high efficiency broadband rectenna for ambient wireless energy harvesting," *IEEE Trans. Antennas Propag*., vol. 63, no. 8, pp. 3486–3495, Aug. 2015.

[16] C. Song, Y. Huang, J. Zhou, and P. Carter, "Improved ultrawideband rectennas using hybrid resistance compression technique," *IEEE Trans. Antennas Propag*., vol. 65, no. 4, pp. 2057–2062, Apr. 2017.

[17] P. Lu, X. S. Yang, J. L. Li, and B. Z. Wang, "A compact frequency reconfigurable rectenna for 5.2- and 5.8-GHz wireless power transmission," *IEEE Trans. Power Electron*., vol. 30, no. 11, pp. 6006–6010, Nov. 2015.

[18] M. Piñuela, P. D. Mitcheson and S. Lucyszyn, "Ambient RF Energy Harvesting in Urban and Semi-Urban Environments," *IEEE Trans. Microw. Theory Tech*., vol. 61, no. 7, pp. 2715-2726, July 2013.

[19] S. Hemour and K. Wu, "Radio-frequency rectifier for electromagnetic energy harvesting: development path and future outlook," *Proc. IEEE*, vol. 102, no. 11, pp. 1667–1691, Nov. 2014.

[20] S. Shen, Y. Zhang, C. Chiu and R. Murch, "An Ambient RF Energy Harvesting System Where the Number of Antenna Ports Is Dependent on Frequency," *IEEE Trans. Microw. Theory Tech*., in press, 2019.

[21] U. Olgun, C.-C. Chen, and J. L. Volakis, "Design of an efficient ambient WiFi energy harvesting system," *IET Microw. Antennas Propag.*, vol. 6, no. 11, pp. 1200–1206, Nov. 2012.

[22] X. Zhang et al., "Two-dimensional MoS2-enabled flexible rectenna for Wi-Fi-band wireless energy harvesting," *Nature*, vol. 566, pp. 368–372, Jan. 2019.

[23] Y. Hu, S. Sun, H. Xu and H. Sun, "Grid-Array Rectenna With Wide Angle Coverage for Effectively Harvesting RF Energy of Low Power Density," *IEEE Trans. Microw. Theory Tech*., vol. 67, no. 1, pp. 402-413, Jan. 2019.

[24] E. Vandelle, D. H. N. Bui, T. Vuong, G. Ardila, K. Wu and S. Hemour, "Harvesting Ambient RF Energy Efficiently With Optimal Angular Coverage," *IEEE Trans. Antennas Propag*., vol. 67, no. 3, pp. 1862-1873, March 2019.

[25] J. A. Hagerty, et.al, "Recycling ambient microwave energy with broad-band rectenna arrays," *IEEE Trans. Microw. Theory Tech*., vol. 52, no. 3, pp. 1014-1024, March 2004.

[26] C. Song et al., "Matching network elimination in broadband rectennas for high-efficiency wireless power transfer and energy harvesting," *IEEE Trans. Ind. Electron.*, vol. 64, no. 5, pp. 3950–3961, May 2017.

[27] C. Song, Y. Huang, P. Carter, J. Zhou, S. Joesph and G. Li, "Novel Compact and Broadband Frequency-Tunable Rectennas with Adaptive Input-Power and Load Impedance Range," *IEEE Trans. Antennas Propag*., vol. 66, no. 7, pp. 3306-3316, Jul. 2018.

[28] C. Song, et al., "A Novel Quartz Clock with Integrated Wireless Energy Harvesting and Wireless Sensing for Smart Home Applications," *IEEE Trans. Industrial Electronics*., vol. 66, no. 5, pp. 4042 - 4053, Apr. 2019.

[29] H. Liu, Y. Liu, W. Zhang and S. Gao, "An Ultra-Wideband Horizontally Polarized Omnidirectional Circular Connected Vivaldi Antenna Array," *IEEE Trans. Antennas Propag*., vol. 65, no. 8, pp. 4351-4356, Aug. 2017.

[30] Online-Available:https://www.cypress.com/documentation/development-kitsboards/s6sae101a00sa1002-solar-powered-iot-device-kit

[31] Y. Wang and S. Chung, "A Short Open-End Slot Antenna With Equivalent Circuit Analysis," *IEEE Trans. Antennas Propag.*, vol. 58, no. 5, pp. 1771-1775, May 2010.

[32] C. Deng and Y. Xie, "Design of Resistive Loading Vivaldi Antenna," *IEEE Antennas and Wireless Propagation Letters*, vol. 8, pp. 240-243, 2009.

[33] A. Boaventura, D. Belo, R. Fernandes, A. Collado, A. Georgiadis and N. B. Carvalho, "Boosting the Efficiency: Unconventional Waveform Design for Efficient Wireless Power Transfer," *IEEE Microwave Magazine*, vol. 16, no. 3, pp. 87-96, April 2015.

[34] S. Shen, Y. Zhang, C. Chiu and R. D. Murch, "A Triple-band High-Gain Multibeam Ambient RF Energy Harvesting System Utilizing Hybrid Combining," *IEEE Trans. Ind. Electron*. In press, Nov. 2019. doi: 10.1109/TIE.2019.2952819.

[35] Y.-J. Ren and K. Chang, "5.8-GHz circularly polarized dual-diode rectenna and rectenna array for microwave power transmission," *IEEE Trans. Microw. Theory Techn*., vol. 54, no. 4, pp. 1495–1502, Jun. 2006.

[36] F. Congedo, G. Monti, L. Tarricone and V. Bella, "A 2.45-GHz Vivaldi Rectenna for the Remote Activation of an End Device Radio Node," *IEEE Sensors Journal*, vol. 13, no. 9, pp. 3454-3461, Sept. 2013.

[37] G.-N. Tan, X.-X. Yang, H. Mei, and Z.-L. Lu, "Study on millimeter-wave Vivaldi rectenna and arrays with high conversion efficiency," *Int. J. Antennas Propag.*, vol. 2016, pp. 1–8, Dec. 2016.

CHAOYUN SONG (M'16) received BEng. MSc and PhD degrees in electrical engineering and electronics from The University of Liverpool (UoL), Liverpool, UK, in 2012, 2013 and 2017, respectively.

He is currently an Assistant Professor with the School of Engineering and Physical Sciences (EPS), Heriot-Watt University, Edinburgh, Scotland, UK. He was a Postdoctoral Research Associate with UoL between 2017 and 2020. He has published more than 70 papers (including 30 IEEE transactions) in peer-reviewed journals and conference proceedings. He has held 2 US patents and 2 UK patents. His current research interests include wireless energy harvesting and wireless power transfer technologies, antennas and microwave circuits using novel materials, dielectric material and ionic liquids in RF applications, metamaterials and meta-surfaces in RF, energy harvesting and sensing technologies.

Dr. Song was the recipient of many international awards such as the BAE Systems Chairman's Award in 2017 for the innovation of next generation global navigation satellite system antennas. In 2018, he received the highly-commended award from the prestigious IET Innovation Awards over three categories – "Energy and Power", "Emerging Technologies" and "Young Innovators". Dr. Song has been a regular Reviewer of more than 25 international journals including Nature Communications, Applied Physics Letters, Nano Energy and seven IEEE transactions and a Guest Editor for Wireless Communications and Mobile Computing.

PING LU (M'18) received the B.S. degree in electrical engineering and automation from Southwest Jiaotong University, Chengdu, China, in 2012. She received the Ph.D. degrees degree in radio physics from the University of Electronic Science and Technology, Chengdu, 2018. From 2015 to 2017, she was a Joint Ph.D. Student Scholar at the Laboratoire Ampére, École Centrale de Lyon, INSA de Lyon, Université Claude Bernard de Lyon, Villeurbanne, France. She is currently an Assistant Professor with the School of Electronics and Information Engineering, Sichuan University. Her current research interests include rectenna, non-diffraction beams, and wireless power transmission.

SHANPU SHEN (S'15-M'18) received the bachelor's degree in communication engineering from the Nanjing University of Science and Technology, Nanjing, China, in 2013, and the Ph.D. degree in electronic and computer engineering from The Hong Kong University of Science and Technology (HKUST), Hong Kong, in 2017.

He was a Visiting Ph.D. Student with the Microsystems Technology Laboratories, Massachusetts Institute of Technology, Cambridge, MA, USA, in 2016. He was a Post-Doctoral Fellow with HKUST from 2017 to 2018 and he was a Post-Doctoral Research Associate with the Communications and Signal Processing Group, Imperial College London, London, UK, from 2018 to 2020. He is currently a Research Assistant Professor with HKUST.

His current research interests include RF energy harvesting, wireless power transfer, MIMO systems, and antenna design and optimization.